

~~CONFIDENTIAL~~

# RESEARCH MEMORANDUM

SOME EFFECTS OF FLOW SPOILERS AND OF AERODYNAMIC BALANCE  
ON THE OSCILLATING HINGE MOMENTS FOR A SWEPT FIN-RUDDER  
COMBINATION IN A TRANSONIC WIND TUNNEL

By Robert W. Herr, Frederick W. Gibson,  
and Robert S. Osborne

Langley Aeronautical Laboratory  
Langley Field, Va.

CLASSIFIED DOCUMENT

This material contains information affecting the National Defense of the United States within the meaning of the espionage laws, Title 18, U.S.C., Secs. 793 and 794, the transmission or revelation of which in any manner to an unauthorized person is prohibited by law.

**NATIONAL ADVISORY COMMITTEE  
FOR AERONAUTICS**

WASHINGTON

May 28, 1958

~~CONFIDENTIAL~~

NACA RM L58C28

CLASSIFICATION CHANGES

NASA CCN 80 dtd 10/13/06



## NATIONAL ADVISORY COMMITTEE FOR AERONAUTICS

## RESEARCH MEMORANDUM

SOME EFFECTS OF FLOW SPOILERS AND OF AERODYNAMIC BALANCE  
ON THE OSCILLATING HINGE MOMENTS FOR A SWEPT FIN-RUDDER  
COMBINATION IN A TRANSONIC WIND TUNNEL

By Robert W. Herr, Frederick W. Gibson,  
and Robert S. Osborne

## SUMMARY

Force-oscillation tests were made in the Langley 8-foot transonic pressure tunnel to investigate some effects of an overhang-type aerodynamic balance and of a flow spoiler on the dynamic hinge-moment characteristics of a full-span flap-type rudder on a 5-percent-thick, swept vertical fin of low aspect ratio. Tests were made over a Mach number range of 0.60 to 1.20 at a constant oscillating amplitude of  $\pm 2.5^\circ$ . The range of reduced frequencies (based on the average semichord of the rudder) varied from 0.005 to 0.067. Tunnel stagnation pressures were 0.25, 0.40, and 0.70 atmosphere.

Test results show that the aerodynamic damping moment on the plain rudder becomes unstable near a Mach number of 0.975 and remains unstable to the maximum speed of the tests ( $M = 1.20$ ). The addition of the aerodynamic balance to the rudder moved the aerodynamic damping coefficient into the stable region at these Mach numbers, whereas the addition of the strip spoiler moved the aerodynamic damping coefficient still farther into the stable region. The aerodynamic spring coefficient varied only slightly with reduced frequency over the Mach number and frequency ranges covered. The aerodynamic damping coefficient was also essentially independent of reduced frequency except near a Mach number of 0.95.

## INTRODUCTION

As airplanes began to fly at transonic speeds, the phenomenon of "aileron buzz" or single-degree-of-freedom flutter of the control surface was encountered with increasing frequency. Some of the early work on this phenomenon (refs. 1 and 2) indicated that the occurrence of this type of flutter might depend on several geometric parameters. However,

~~CONFIDENTIAL~~

as higher speed airplanes have evolved, the problem of aileron buzz has persisted and in most cases some form of additional structural damping has been required to permit operation of the airplane throughout its capabilities. In a few cases, satisfactory aerodynamic modifications have been found which have eliminated the need for control surface dampers.

The purpose of the present investigation is to determine the aerodynamic hinge moments acting on the oscillating rudder of a typical thin swept tail with particular interest in the effects of the addition of an aerodynamic balance and of a small spoiler. The tests were performed in the Langley 8-foot transonic pressure tunnel and covered the Mach number range from 0.60 to 1.20. The effects of Reynolds number were studied briefly by testing at stagnation pressures of 0.25, 0.40, and 0.70 atmosphere.

#### SYMBOLS

$C_h$	control hinge-moment coefficient, $\frac{\text{Hinge moment}}{2M'q}$
$M_\delta$	aerodynamic hinge moment on control per unit deflection, ft-lb/radian
<hr/>	
$q$	free-stream dynamic pressure, lb/sq ft
$M'$	area moment of rudder area rearward of and about hinge line, 0.1152 ft <sup>3</sup>
$c$	total rudder chord measured at midspan of control, ft
$\bar{c}$	mean aerodynamic chord of fin and rudder, 1.65 ft
$k$	reduced frequency, $\frac{\omega c}{2V}$
$\omega$	angular frequency of oscillation, radians/sec
$V$	free-stream velocity, ft/sec
$M$	Mach number

$$\left. \begin{aligned} C_{h\delta, \omega} &= \frac{\text{Real part of } M_{\delta}}{2M'q}, \text{ per radian} \\ C_{h\dot{\delta}, \omega} &= \frac{\text{Imaginary part of } M_{\delta}}{2M'qk}, \text{ per radian} \end{aligned} \right\} \begin{array}{l} \text{subscript } \omega \text{ indicates} \\ \text{coefficients that are} \\ \text{a function of } \omega \end{array}$$

$S_{\delta}$  static mass unbalance of rudder about hinge line, ft-lb

$I_{\delta}$  mass moment of inertia of rudder about hinge line, lb-ft<sup>2</sup>

### APPARATUS AND METHOD

During tunnel operations the rudder on the test configuration was mechanically driven in sinusoidal motion at constant amplitude and at various frequencies. The total (aerodynamic, inertial, and small elastic) oscillating hinge moments developed by the rudder were obtained from the calibrated response of strain gages mounted on a strain-gage balance which was part of the rudder driving shaft. The strain-gage response was separated into components in phase and 90° out of phase with the rudder displacement by means of a resolver technique which will be described later.

#### Model

The model tested was a swept fin with full-span rudder mounted on a half body and attached to the wall of the Langley 8-foot transonic pressure tunnel, as shown in figure 1. Dimensional details of the fin and rudder are given in figure 2. The rudder hinge line was located at the 75-percent-chord station and was swept back 35°. The fin-rudder panel (or exposed) aspect ratio was 1.08, the taper ratio was 0.5, and airfoil sections were NACA 65A005. The fin was of relatively stiff steel skin construction in order to keep the fundamental bending frequency well above the driving frequency. Similarly, the rudder was designed to have a high torsional stiffness with a low inertia about the hinge line to reduce the amount of dynamic structural twist of the rudder at the higher driving frequencies. As indicated in figure 3(a), the rudder stiffness was concentrated in a solid-steel leading edge. The rear section of the rudder consisted of balsa wood glued to both sides of a magnesium insert, the whole of which was covered with plastic impregnated fiber glass.

The three rudder test configurations are illustrated in figure 3(a). Configuration 1 consisted of the plain 25-percent-chord rudder with mass balance. A photograph of the rudder with the steel balance weights

~~CONFIDENTIAL~~

attached is presented in figure 3(b). These mass balances were considered to contribute little aerodynamic balance relative to configuration 2. The area and area moment rearward of the hinge line in configuration 1 were 99 sq in. and 199 in.<sup>3</sup>, respectively. For configuration 2, aerodynamic balance was provided by a round nose overhang, the plan-form dimensions of which are given in figure 3(c). The ratio of the plan-form area ahead to the area rearward of the hinge line was 0.473. Configuration 3 was identical to configuration 1 except that flow spoilers were added at the 25-percent-chord line of the rudder. These spoilers consisted of 1/8-inch-square balsa strips glued to both surfaces and extending the full span of the rudder. The height of each spoiler was, then, 0.63 percent of the fin-rudder mean aerodynamic chord.

The rudder was attached to the fin at three points by means of flex spring pivots as shown in figure 2. This type of hinge was chosen because previous experience had shown them to be superior for this type of use. Although the flex-type hinge adds some structural damping and spring force to the system, these forces have been found to be relatively small and constant.

The rudder weight, center of gravity, unbalance, and inertia are given in the following table. These weights and inertias include the rudder shaft inboard to the strain-gage balance.

Configuration	Weight, lb	Center of gravity, ft	$S_{\delta}$ , ft-lb	$I_{\delta}$ , lb-ft <sup>2</sup>
1	10.36	0.00375	0.0375	0.0705
2	9.97	.00340	.034	.0732
3	10.36	.00375	.0375	.0705

As may be seen, all three configurations were nearly statically mass balanced about the hinge line.

The driving mechanism is illustrated in figure 4. The mechanism consisted essentially of a direct-current drive motor and shaft with an eccentric and crank to convert rotary motion to reciprocating motion. A secondary motor-generator set, not shown in the figure, was used in conjunction with the drive motor to control the frequency of oscillation.

#### Tunnel and Model Support

The Langley 8-foot transonic pressure tunnel is a single-return, rectangular, slotted-throat wind tunnel having controls that allow for

the independent variation of Mach number, stagnation pressure, temperature, and humidity.

Unpublished results of previous tests have indicated that the total boundary-layer thickness on the tunnel wall in the vicinity of the model varied from 3.5 inches at a Mach number of 0.60 to 3.0 inches at Mach numbers above 0.90 for the range of stagnation pressures of the present tests. In an effort to get more of the fin-rudder panel outside the boundary layer, the model was mounted on a half body which extended 4.75 inches out from the tunnel wall and was 100 inches long. (See figs. 1 and 2.) The half body consisted of a straight flat portion extending from the leading edge of the fin-rudder root chord to the trailing edge of the tip chord and a circular-arc forebody and afterbody. Tests indicated that the total boundary-layer thickness on the flat portion of the body varied linearly with Mach number from 3.2 inches at a Mach number of 0.60 to 2.0 inches at a Mach number of 1.2. Mounting the fin-rudder panel on the half body appeared to have no great advantage over a wall-type mounting since the total boundary-layer thickness along the fin-rudder root was reduced only an average of 0.6 inch (approximately 3 percent of the model span) over the Mach number range.

An analysis of the supersonic boundary-reflected disturbance patterns in the vicinity of the model indicated that the reflected shock wave from the nose of the half body probably intersected the fin-rudder panel at Mach numbers from approximately 1.05 to 1.10.

### Instrumentation

Separation of the rudder hinge moments in phase with the rudder angular position (real) and the rudder angular velocity (imaginary) was accomplished by a resolver technique which is illustrated in the block diagram of figure 5. The oscillator supplies a 3-kilocycle voltage to the strain-gage-bridge circuit. When the torque is oscillatory, the resulting output signal is an amplitude modulated 3-kilocycle voltage whose modulation frequency is that of the applied torque. The signal is then amplified by the linear amplifier and passed through a resolver. The resolver is essentially a rotary transformer having two secondary windings wound at right angles to each other on a rotor. The flux linkage of the rotor windings, and hence the transformer ratio, is proportional to the sine of the angle that the windings make with the flux produced by the primary winding current. Passing a carrier signal through the resolver therefore gives the product of the signal times  $K_2(\sin \omega t)$  at one set of terminals and the signal times  $K_2'(\sin \omega t)$  at the other set of terminals (where  $K_2$  and  $K_2'$  are arbitrary constants). A very stiff drive system between the resolver and the strain-gage bridge made it possible to orientate the resolver so as to produce a voltage from

one secondary output winding inphase with the rudder position. The voltage from the remaining secondary winding lags by  $90^\circ$  and is, hence, inphase with the rudder velocity. The individual outputs are amplified and then demodulated to remove the 3-kilocycle carrier frequency from the signal. The resulting output currents are then read on heavily damped direct-current microammeters to obtain the average value of each component.

Calibration constants for the system were determined from static tests and from wind-off tests. In the static tests microammeter readings were taken with static moments applied to the shaft for each of the two resolver settings - one at zero rudder amplitude and the other at maximum rudder amplitude. The calibration constants thus obtained were checked by securing a known inertia to the shaft and taking readings at various driving frequencies at constant amplitude.

A resistance wire strain gage was mounted near the root of the fin as shown in figure 2. The output of this strain gage during the tunnel tests was recorded on an oscillograph as an indication of the relative bending moments.

### Tests

The model was tested at an angle of attack of  $0^\circ$  at Mach numbers from 0.60 to 1.2 and tunnel stagnation pressures of 0.25, 0.40, and 0.70 atmosphere. The test Reynolds number based on a fin-rudder mean aerodynamic chord of 1.65 feet varied from  $1.40 \times 10^6$  to  $4.95 \times 10^6$  as shown in figure 6. The rudder hinge moments were measured at a constant amplitude of  $\pm 2.5^\circ$  over a frequency range from 5 to 35 cps. Because the resonant bending frequency of the fin was 50 cps, the rudder frequency was limited to 35 cps in order to insure the safety of the model and tunnel. At a given tunnel density, the real and imaginary components of the rudder hinge moments were measured over the range of frequencies at several Mach numbers. The following table gives the test conditions for the three model configurations:

Configuration	Stagnation pressure, atm	Mach number range	Frequency range, cps
1	0.25	0.9 to 1.2	5 to 35
	.4	0.6 to 1.2	5 to 35
	.7	0.6 to 1.2	5 to 35
2	.25	0.6 to 1.2	5 to 35
3	.25	0.925 to 1.2	5 to 35
	.7	0.9 to 1.2	5 to 35

The resonant bending frequency of the fin-rudder combination and the torsional frequency of the rudder and drive mechanism were obtained with the use of an air-jet shaker which is described in reference 3. These frequencies for configuration 1 (mass balance only) were 50.1 cps and 175 cps, respectively. The maximum driving frequency of 35 cps being only 1/5 of the rudder natural frequency indicates that the wind-up or structural twist along the span of the rudder would be small. This is borne out in figure 7 which shows the dynamic amplification of the system for driving frequencies up to 50 cps. The dynamic amplification at the rudder midspan at 35 cps is 3.3 percent. The dynamic amplification of the rudder through the frequency range was determined by the use of a mirror and point-source light system in which the mirror was placed on the hinge line at various points along the span.

Measurements were also made at zero airspeed to obtain the tare hinge moments as well as to check on the instrumentation and the structural integrity of the model and rudder hinges.

#### Reduction of Data

The measured hinge moments include not only the desired aerodynamic moments but also an inertia component 180° out of phase with the displacement and small hinge damping and spring components inphase with the velocity and displacement, respectively. The aerodynamic spring and damping moments were obtained by vectorially subtracting the tare moments (zero airspeed) from the total spring and damping moments of the wind-on tests at corresponding frequencies. In some cases the tare hinge moments were large in comparison with the aerodynamic hinge moments. An indication of the relative size of the tare and aerodynamic hinge moments is shown in figure 8 where the tare component and aerodynamic spring components are plotted as a function of frequency for several test conditions.

As mentioned previously, the dynamic amplification of the rudder motion at the maximum driving frequency was 3.3 percent and since the fundamental bending frequency was well above the driving frequency, the hinge-moment coefficients were computed on the basis that the motion involved was pure rotation about the hinge line with no deformation of the control or deflection of the hinge axis.

The hinge moments existing on a linear single-degree-of-freedom system may be represented in complex notation by the relation

$$\frac{M_\delta}{2M'q} = C_{h\delta,\omega}$$

Thus, the spring moment coefficient  $C_{h\delta,\omega}$  and the damping moment coefficient  $C_{h\dot{\delta},\omega}$  were computed by use of the expressions

$$C_{h\delta,\omega} = \frac{\text{Real part of } M_{\delta}}{2M'q}$$

and

$$C_{h\dot{\delta},\omega} = \frac{\text{Imaginary part of } M_{\delta}}{2M'qk}$$

Negative values of  $C_{h\delta,\omega}$  oppose the control displacement and act as an aerodynamic spring which increases the stiffness of the system. Likewise, negative values of  $C_{h\dot{\delta},\omega}$  oppose the control velocity and indicate stable damping.

## RESULTS AND DISCUSSION

The variation of the coefficients  $C_{h\dot{\delta},\omega}$  and  $C_{h\delta,\omega}$  with the reduced-frequency parameter  $k$  is shown in figures 9 to 14 for all test conditions. The data are cross-plotted in figures 15 and 16 to show the effect of Mach number on the hinge moment coefficients at a reduced frequency of 0.025.

### Aerodynamic Damping

Generally speaking, the results shown in figures 9 to 11 indicate only small variation of the damping moment coefficient with reduced frequency at all Mach numbers except near  $M = 0.95$ . In this region the damping coefficient is seen to vary rapidly with the reduced frequency and, for the plain rudder, becomes unstable at the high values of  $k$ .

Effects of flow spoiler.— The effect of the flow spoiler on the aerodynamic damping moments may be seen in figures 9 and 11. At speeds less than  $M = 0.95$  the spoiler adds a small amount of stabilizing damping to that obtained on the plain configuration. At speeds above  $M = 0.95$  the amount of stabilizing damping attributable to the spoiler is increased considerably. At Mach numbers from 1.00 through 1.20 the aerodynamic damping hinge-moment coefficient  $C_{h\dot{\delta},\omega}$  for the plain rudder configuration is unstable throughout the range of the reduced frequency, whereas the damping remained stable for all conditions tested with the flow

spoiler in place. The effect of the spoiler is better illustrated in figure 15 which shows the variation of  $Ch_{\delta,\omega}$  with Mach number at a constant value of  $K = 0.025$ . The abrupt change with Mach number in the damping coefficient near  $M = 0.95$  is still apparent with the spoiler in place. Although no unstable damping moments were encountered with the flow spoiler in place, figures 9 and 11 indicate that at  $M = 0.95$  unstable damping moments would probably have been encountered had it been possible to run at higher values of  $k$ . In addition, it should be pointed out that an investigation of oscillating hinge moments as reported in reference 4 showed the aerodynamic damping coefficient to be nonlinear with amplitude, whereas in the present investigation the oscillations were of constant amplitude.

Effect of aerodynamic balance.— The variation of the aerodynamic damping moment with the reduced-frequency parameter  $k$  for the rudder with aerodynamic balance is shown in figure 9. The range of  $k$  values for this case is somewhat larger due to the greater chord of the control surface. Unlike the flow spoiler, the aerodynamic balance showed a somewhat detrimental effect on the aerodynamic damping at low Mach numbers, although the damping remained stable. At transonic speeds, however, a beneficial effect is noted in that the rudder with aerodynamic balance had stable damping while the plain rudder had unstable damping in this range. The beneficial effect on the damping component is not as pronounced for the aerodynamic balance as was the case for the flow spoiler. This is better illustrated by figure 15 where  $Ch_{\delta,\omega}$  is plotted against Mach number.

#### Aerodynamic Spring

The measured values of the aerodynamic spring were essentially constant with frequency as indicated in figures 12, 13, and 14. These data have been cross plotted and are shown in figures 16 as a function of Mach number for a constant  $k$  of 0.025. For the plain rudder configuration the aerodynamic spring is seen to increase gradually with increasing Mach number until the Mach number of approximately 0.95 is reached, after which the aerodynamic spring coefficient increases much more rapidly with Mach number.

The flow spoiler apparently had but minor effect on the aerodynamic spring at low speeds but at Mach numbers above 0.95 it reduced the restoring moment.

With the aerodynamic balance installed, the control surface was somewhat overbalanced at low speeds. As the center of pressure moves rearward at high speeds, however,  $Ch_{\delta,\omega}$  becomes negative and approaches the values of spring moment obtained with the flow spoiler.

### Control Effectiveness

An acceptable modification to a control surface to eliminate aileron buzz must not only insure stable damping moments throughout the design speed range but also provide satisfactory drag and lift characteristics. In the present tests, no provisions were made to measure these quantities. The output of a strain gage, primarily sensitive to bending moment due to lift, was recorded, however. In figure 17 the output of this gage, at an oscillatory frequency of 5 cps, has been divided by the dynamic pressure and normalized to give a plot roughly proportional to the control effectiveness parameter  $dC_L/d\delta$ . At supersonic speeds it appears that the flow spoiler has reduced the effectiveness of the rudder by the same order of magnitude as the aerodynamic spring moments of figure 16 were alleviated.

### Effects of Reynolds Number

In order to determine some effects of Reynolds number on the aerodynamic spring and damping moments, the plain rudder was tested at three stagnation pressures: 0.25, 0.40, and 0.70 atmosphere. The resulting range of Reynolds numbers as shown in figure 6 is from  $1.4 \times 10^6$  to  $4.95 \times 10^6$ .

The aerodynamic damping moment on the plain rudder is plotted against Mach number in figure 18 at the three stagnation pressures. The effects of Reynolds number for these tests is seen to be small.

### CONCLUSIONS

The results of an investigation at transonic speeds to determine the effects of an overhang-type aerodynamic balance and of a flow spoiler on the oscillating hinge-moment characteristics of a swept, 1/4 chord, full-span control surface oscillating at  $\pm 2.5^\circ$  amplitude indicate the following conclusions:

1. For the plain rudder condition, the aerodynamic damping coefficient was stable at Mach numbers to 0.975 and unstable above this Mach number.
2. The damping coefficients obtained with the flow spoiler in place were stable over the range of parameters tested.
3. The aerodynamic balance produced a stabilizing effect on the damping coefficient above a Mach number of 0.975 but not to as great an extent as did the flow spoiler.

4. The aerodynamic spring coefficient varied only slightly with reduced frequency. The aerodynamic damping coefficient was also essentially independent of reduced frequency except near a Mach number of 0.95.

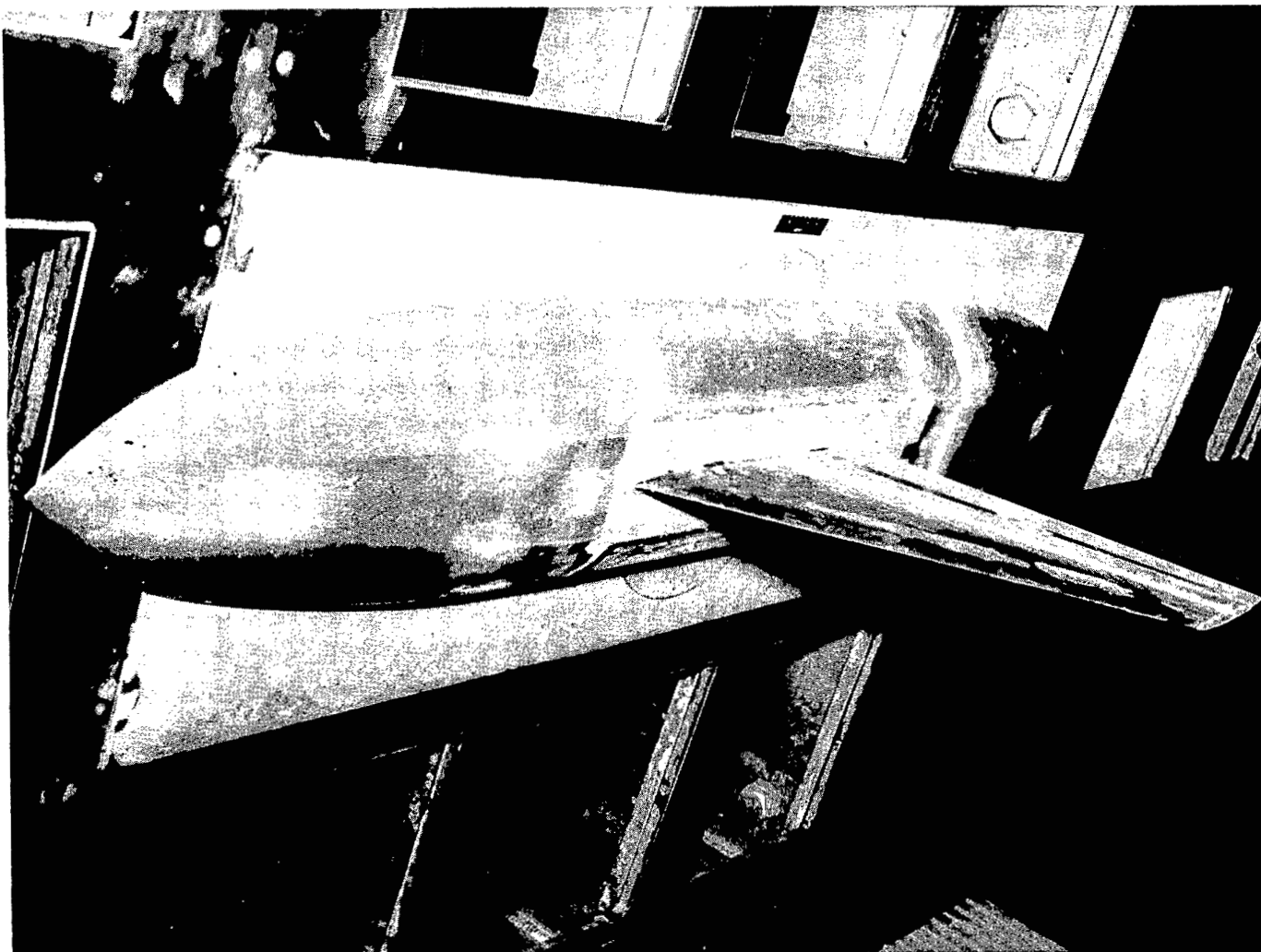
5. For the rudder with flow spoilers, at high speeds the aerodynamic spring moment coefficient and the estimated relative control effectiveness were reduced appreciably.

6. The effects of Reynolds number were indicated to be relatively small over the range of the tests.

Langley Aeronautical Laboratory,  
National Advisory Committee for Aeronautics,  
Langley Field, Va., March 17, 1958.

#### REFERENCES

1. Smilg, Benjamin: The Prevention of Aileron Oscillations at Transonic Airspeeds. Tech. Rep. No. 5530, Army Air Forces, Dec. 24, 1946.
2. Erickson, Albert L., and Stephenson, Jack D.: A Suggested Method of Analyzing for Transonic Flutter of Control Surfaces Based on Available Experimental Evidence. NACA RM A7F30, 1947.
3. Herr, Robert W.: A Wide-Frequency-Range Air-Jet Shaker. NACA TN 4060, 1957.
4. Thompson, Robert F., and Moseley, William C., Jr.: Effect of Hinge-Line Position on the Oscillating Hinge Moments and Flutter Characteristics of a Flap-Type Control at Transonic Speeds. NACA RM L57C11, 1957.



L-57-1835  
Figure 1.- Model mounted on half body in test section of Langley 8-foot  
transonic pressure tunnel.

Exposed area of fin and rudder 395 sq in.  
 Aspect ratio 1.08  
 Taper ratio 0.5  
 Airfoil section parallel  
 to free stream NACA 65A005

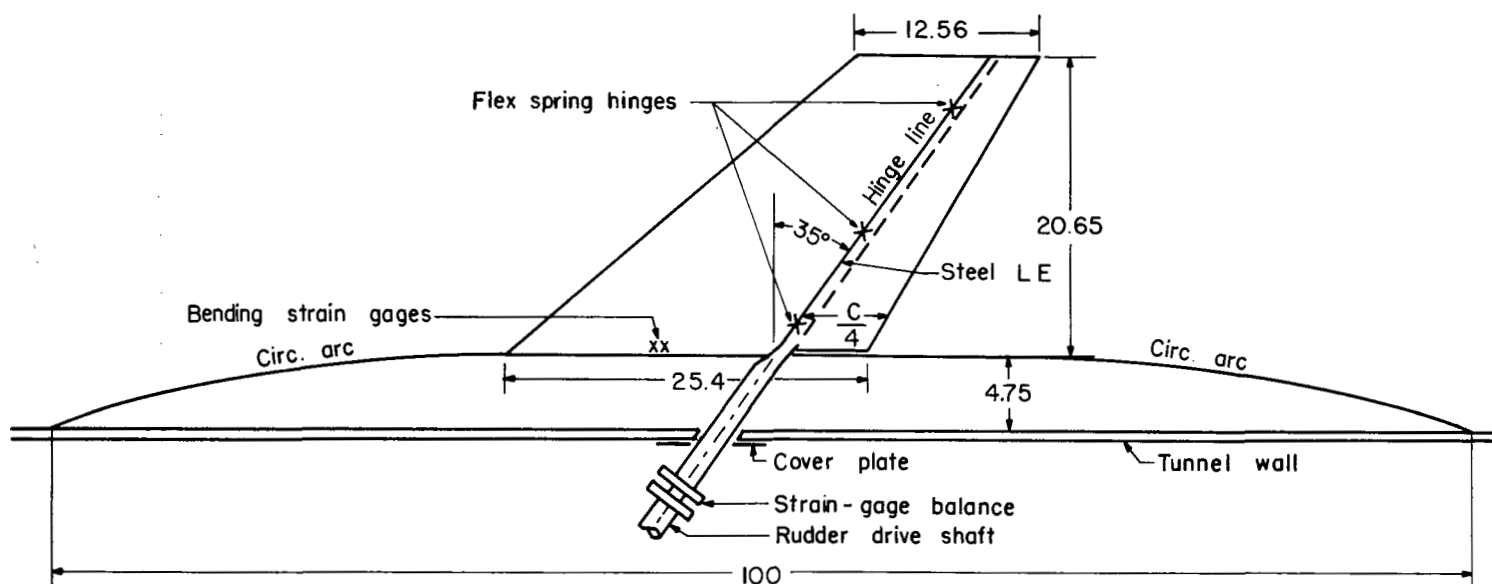
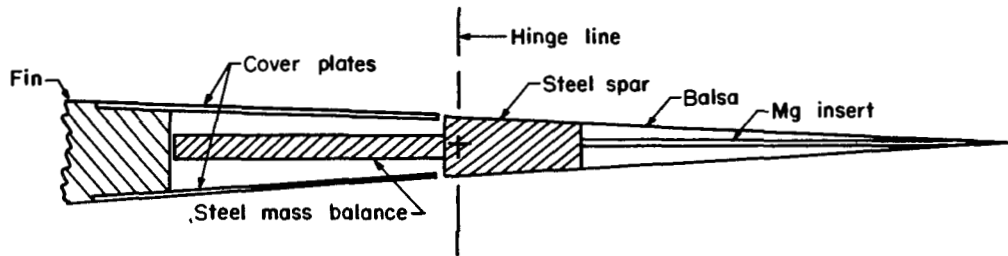
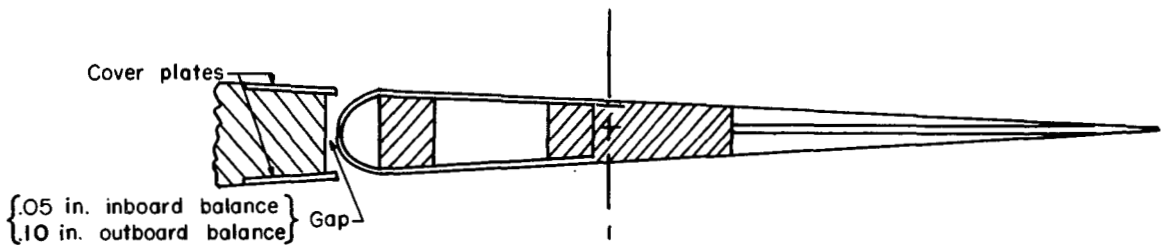


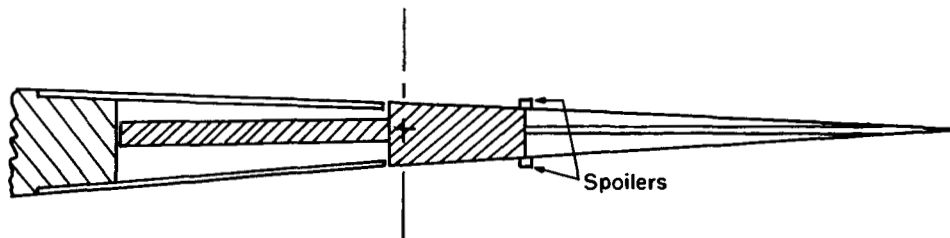
Figure 2.- General dimensions of the test model. All dimensions are in inches.



Configuration 1.- Plain rudder, mass balanced.



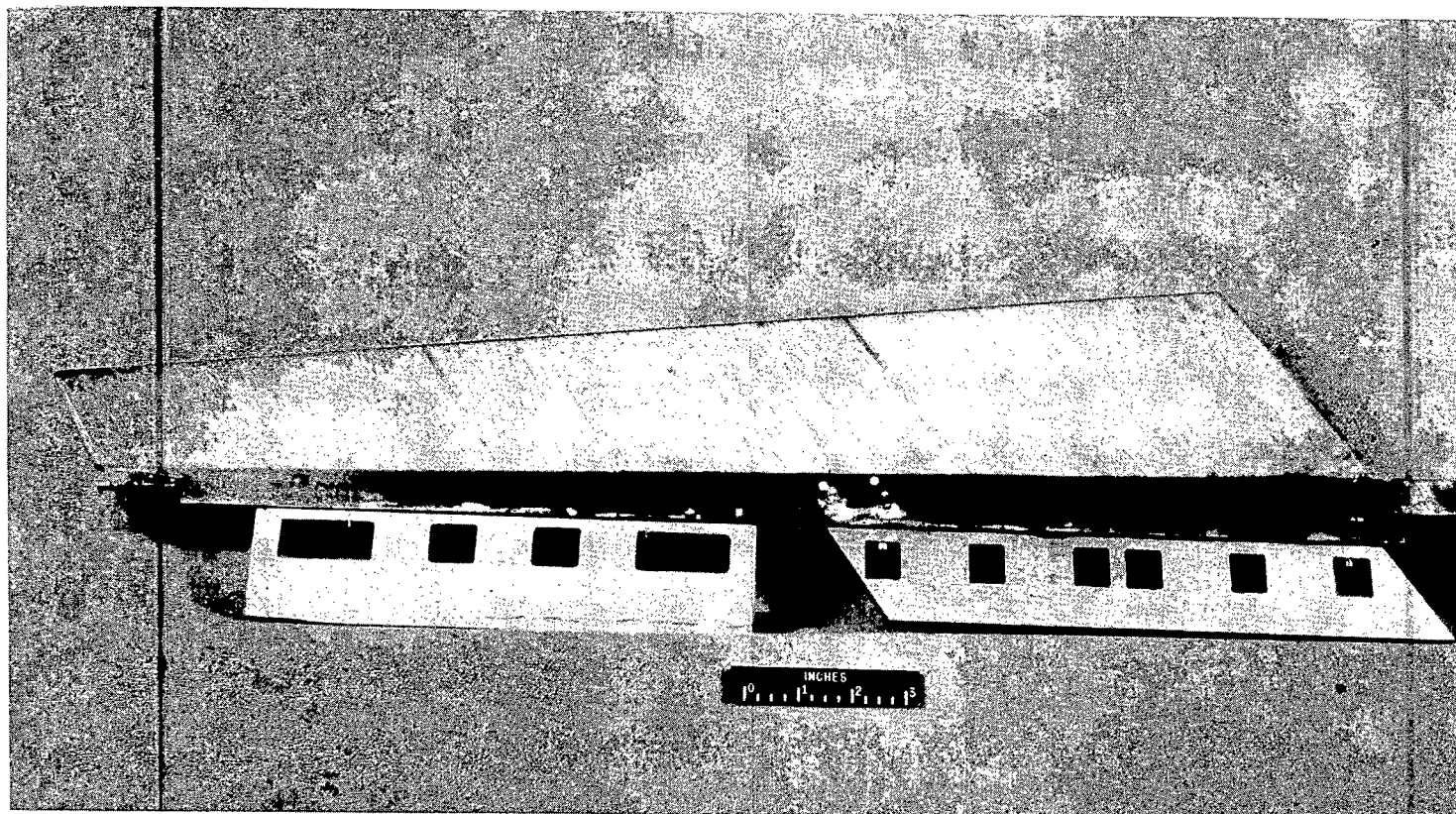
Configuration 2.- Rudder with mass and aerodynamic balance.



Configuration 3.- Mass-balanced rudder with flow spoilers.

(a) Sketch showing the test configurations.

Figure 3.- Model details.

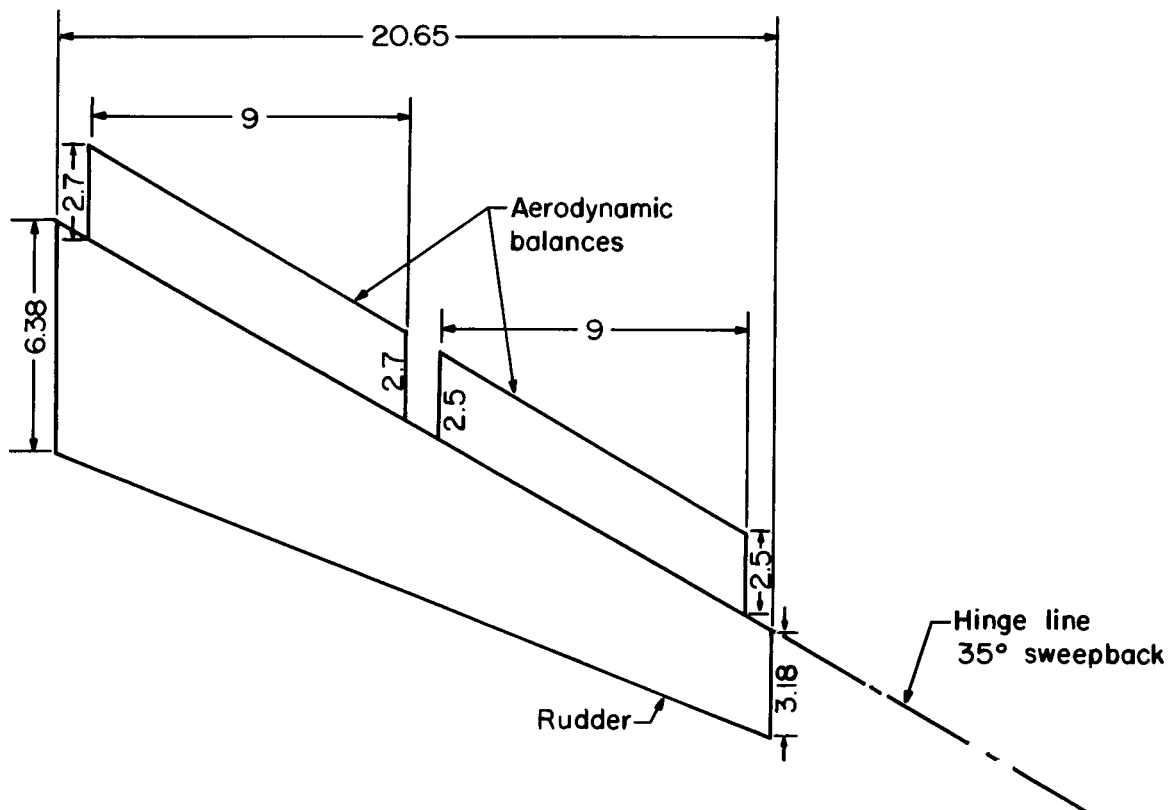


(b) Rudder with mass balances.

L-58-230

Figure 3.- Continued.

	Area	Moment of area about hinge line
Inboard balance	24 sq in.	26.4 cu in.
Outboard balance	22.8 sq in.	23.1 cu in.
Rudder	99.0 sq in.	199 cu in.



(c) General dimensions of the fin and rudder. All dimensions are in inches.

Figure 3.- Concluded.

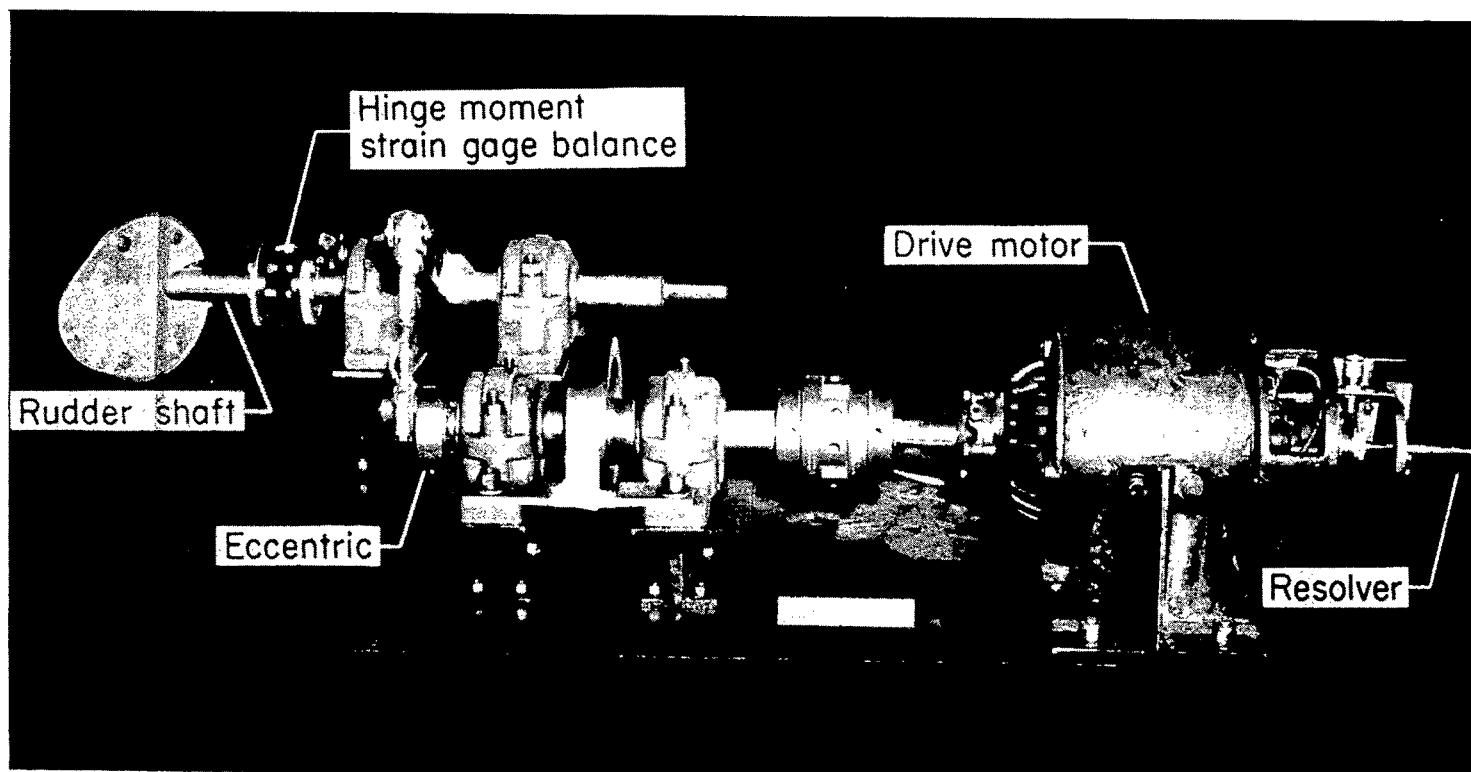


Figure 4.- Model driving mechanism.

L-57-1834.1

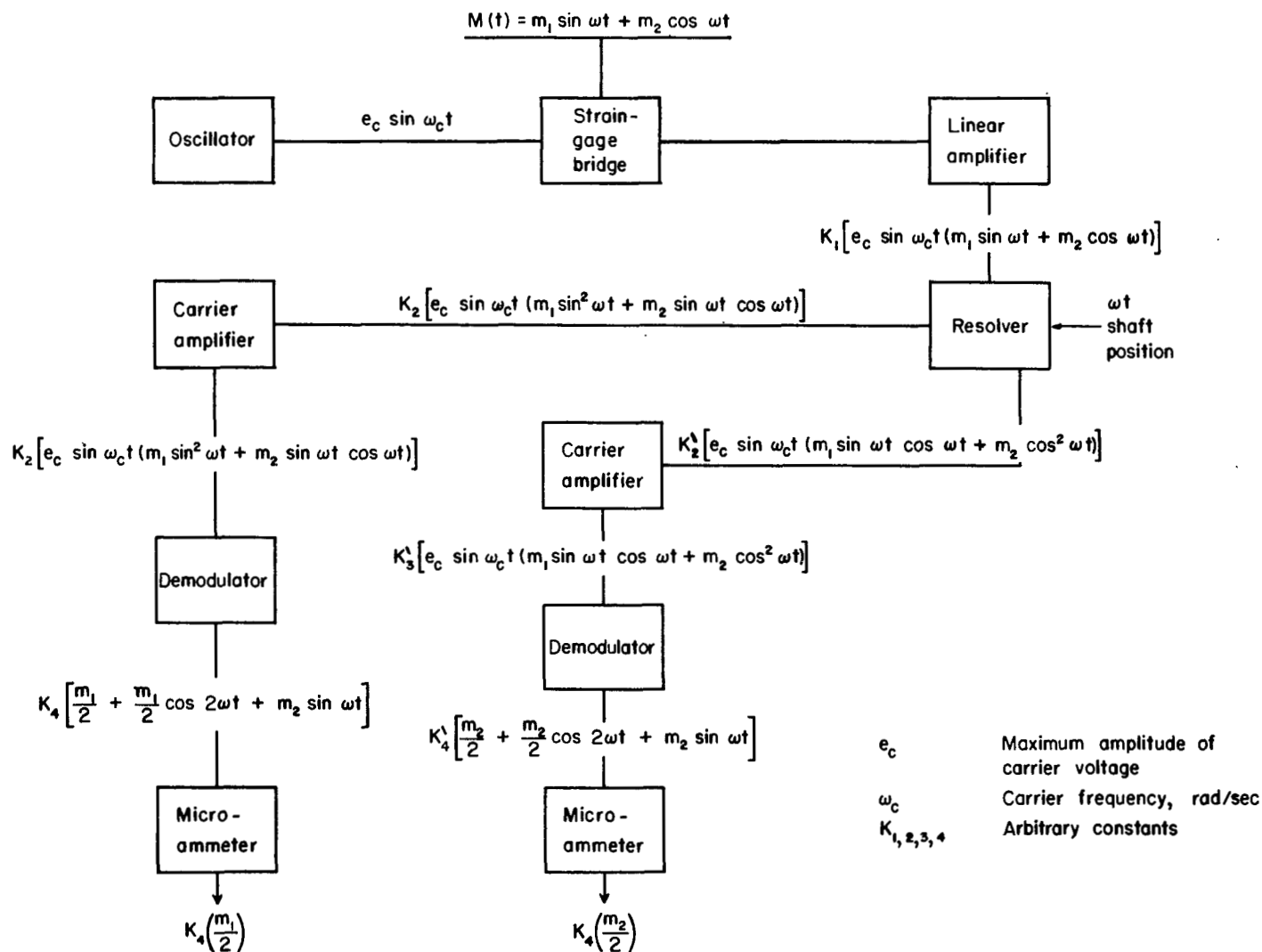


Figure 5.- System used to separate the dynamic hinge moments into the real and imaginary components.

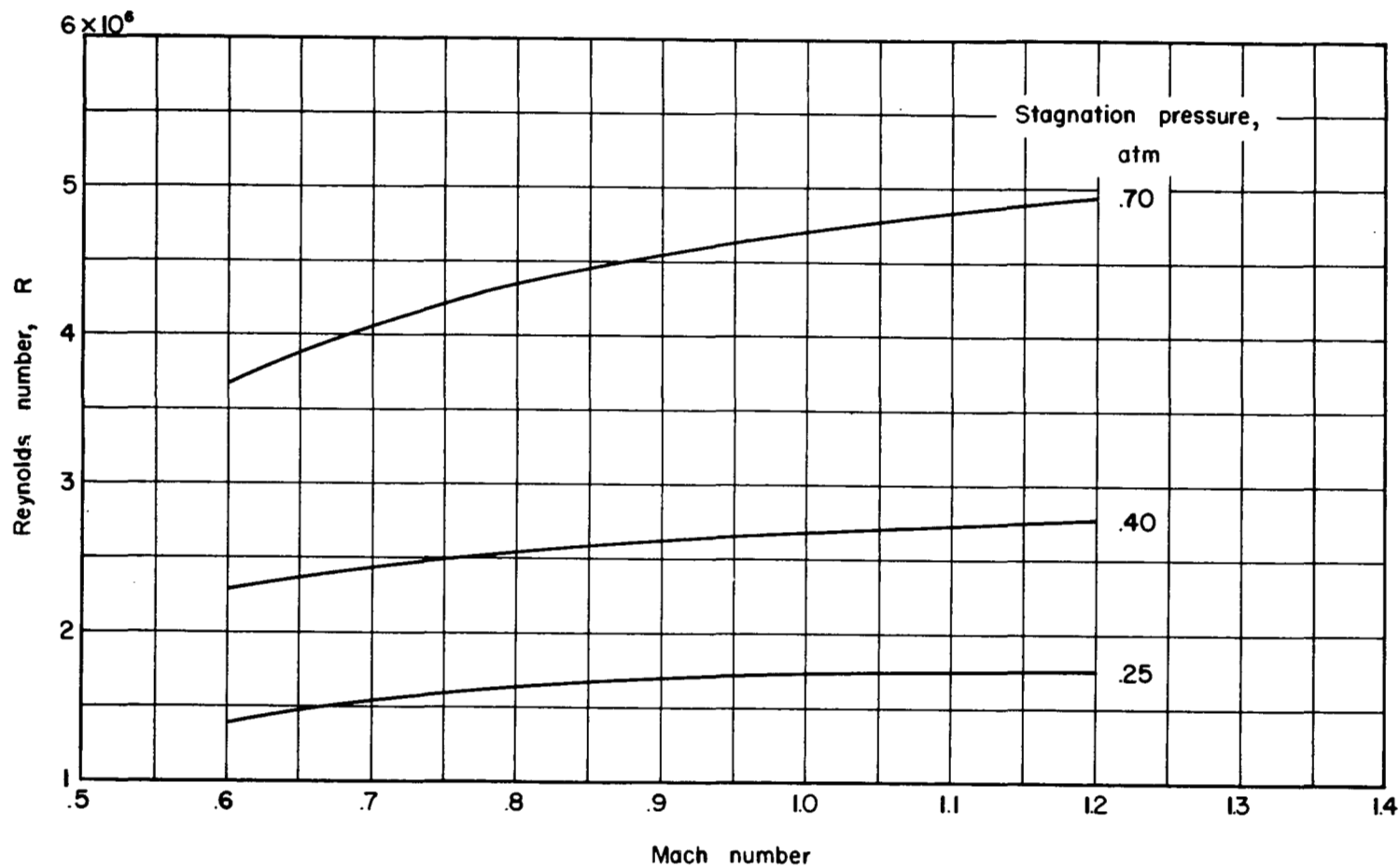


Figure 6.- Variation of test Reynolds number (based on mean aerodynamic chord of 1.65 feet) with Mach number.

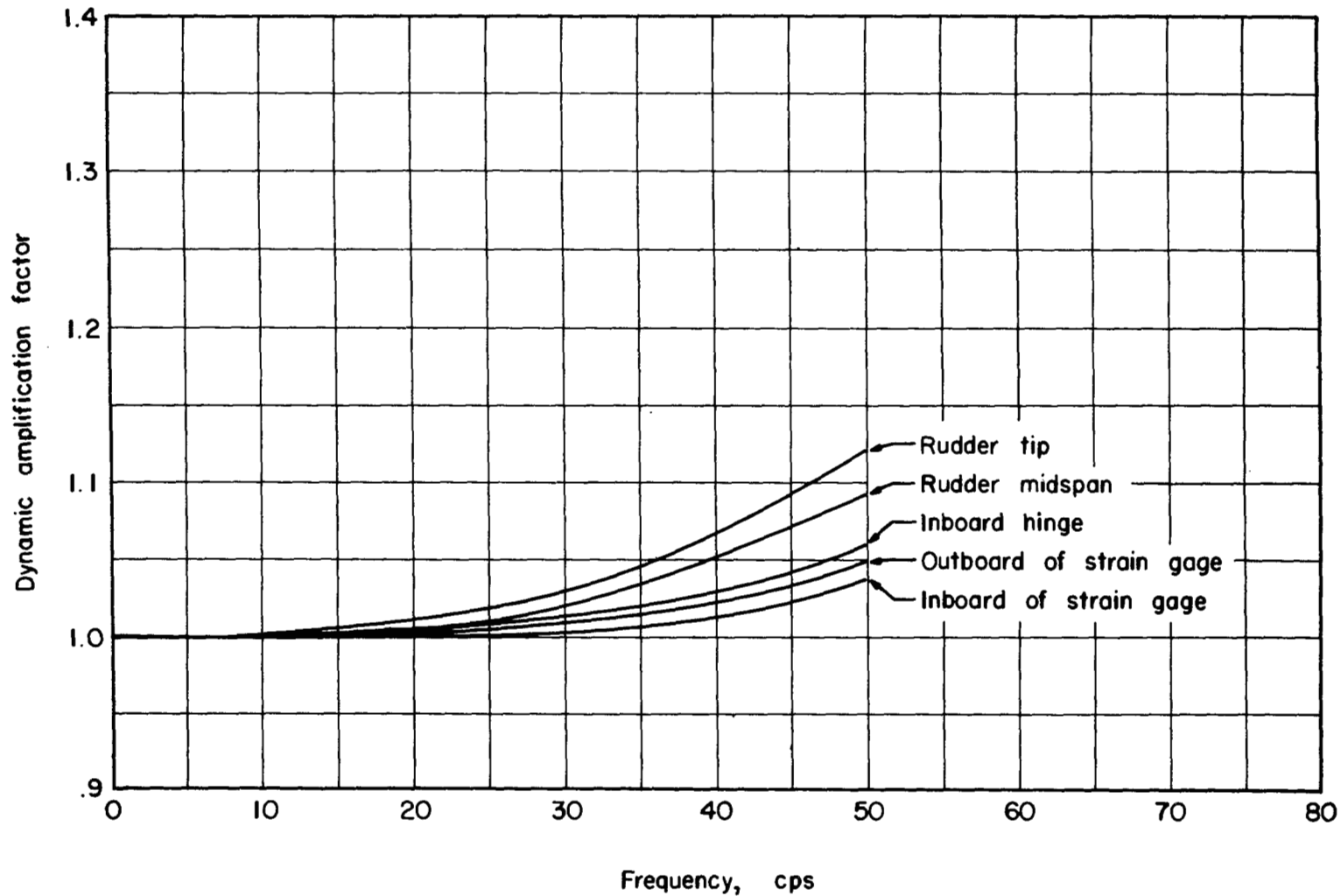


Figure 7.- Dynamic amplification of rudder oscillation amplitude in still air. Plain rudder (configuration 1).

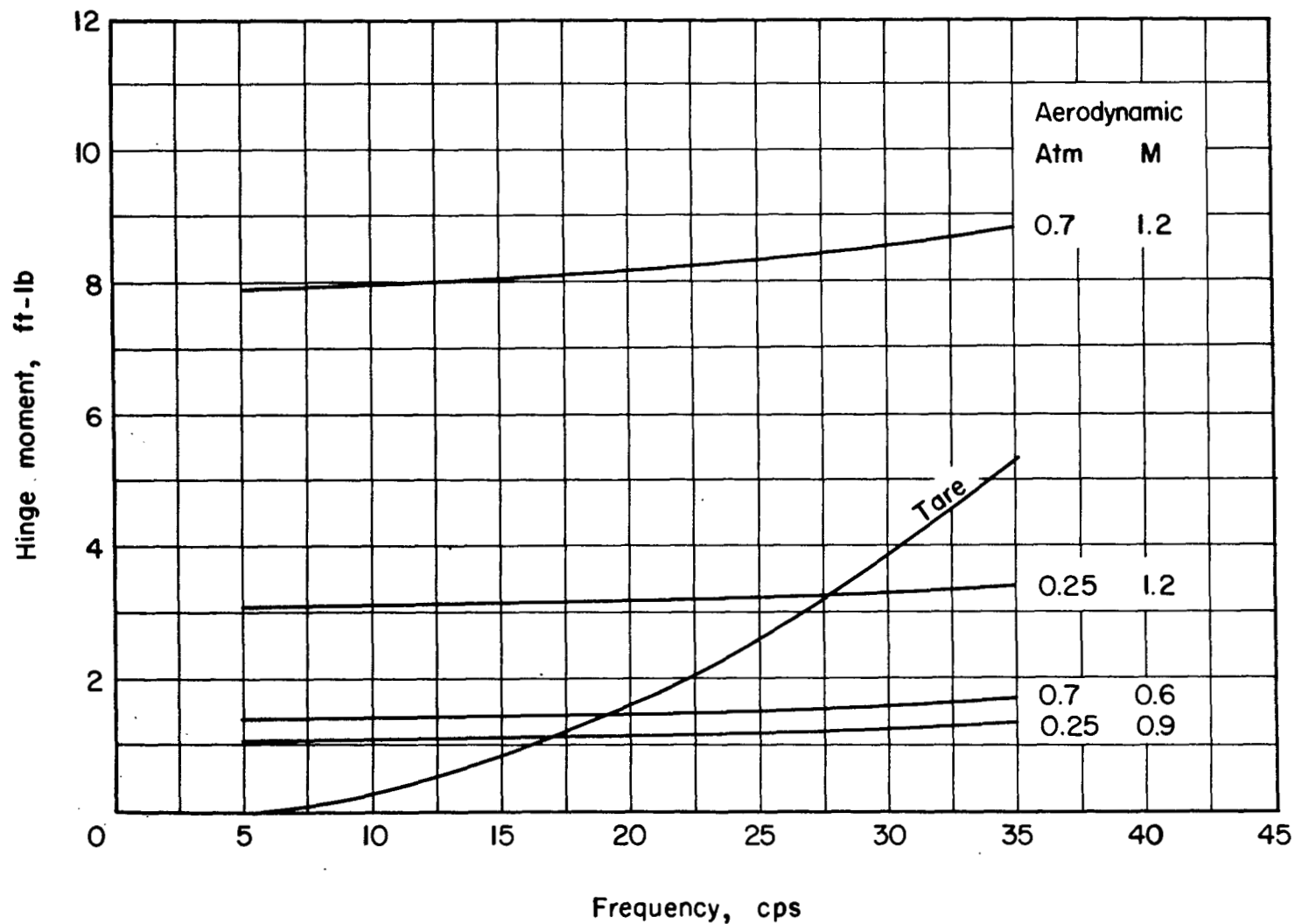


Figure 8.- Comparison of the tare hinge moments with the spring component of the aerodynamic hinge moments at several Mach numbers and stagnation pressures through the frequency range.

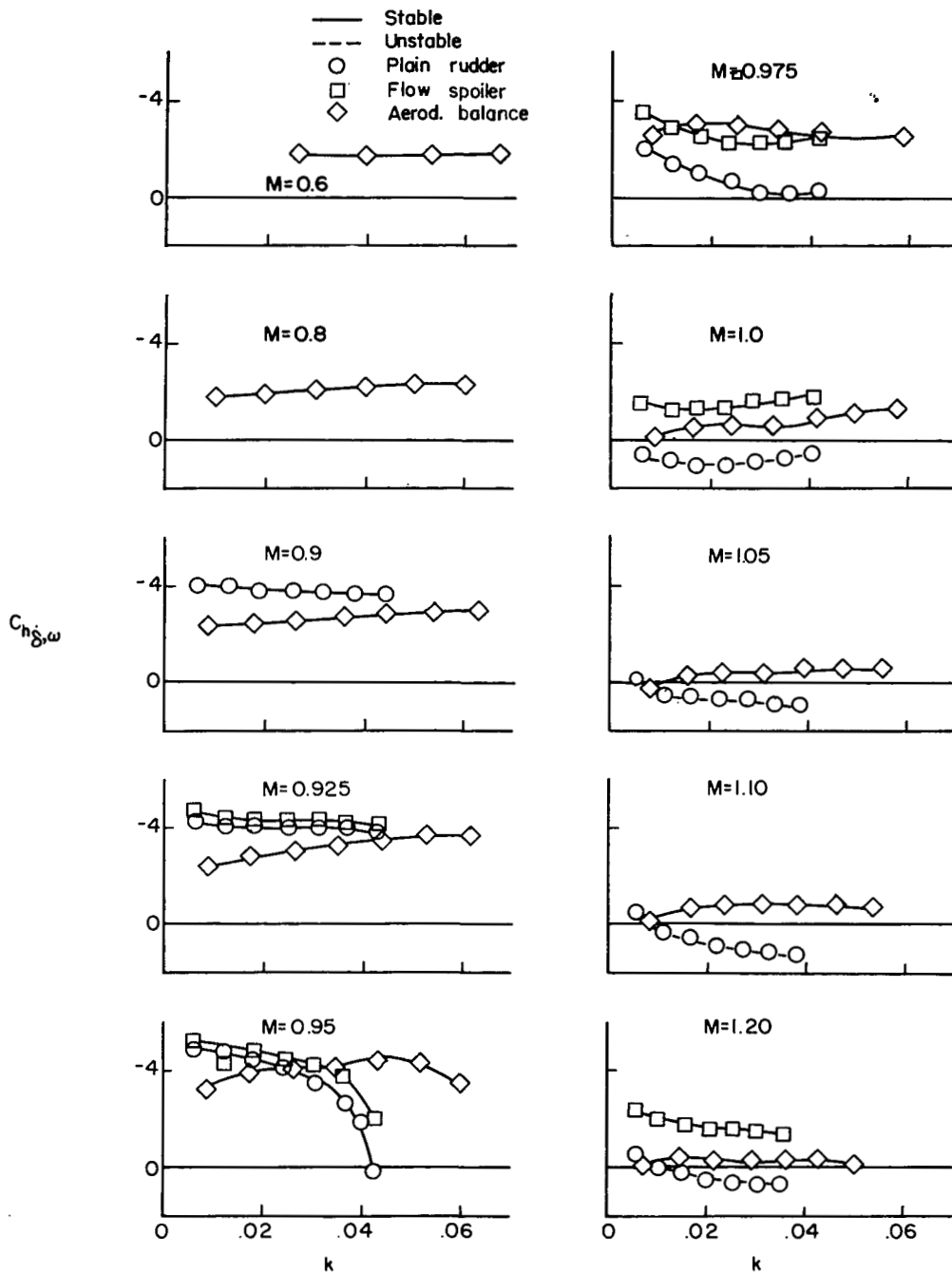


Figure 9.- Variation of  $C_{h_{\delta, \omega}}$  with reduced frequency  $k$  for various Mach numbers showing effect of flow spoilers and aerodynamic balance. Stagnation pressure, 0.25 atmosphere.

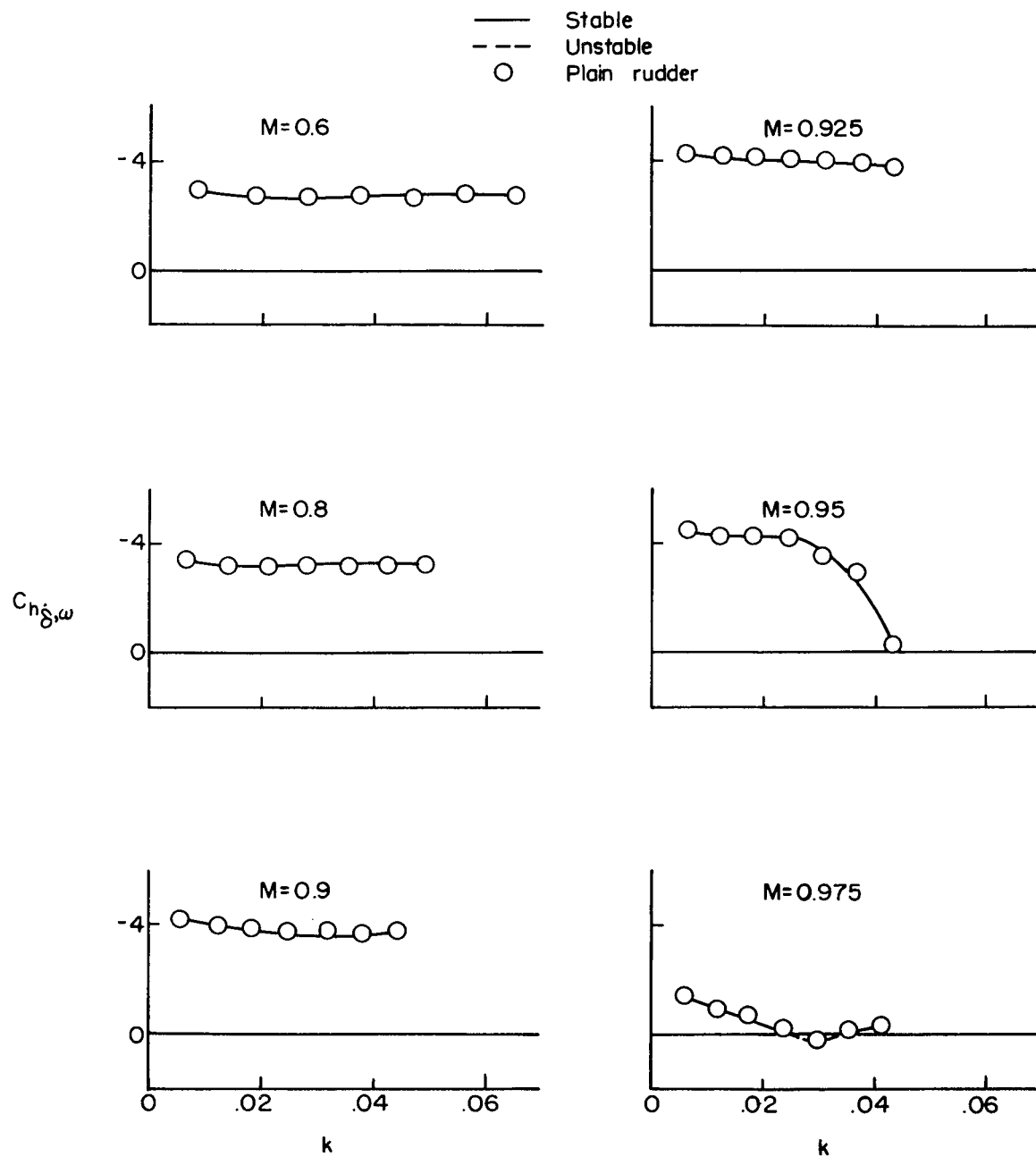


Figure 10.- Variation of  $C_{h\delta, \omega}$  with reduced frequency  $k$  for various Mach numbers. Stagnation pressure, 0.40 atmosphere.

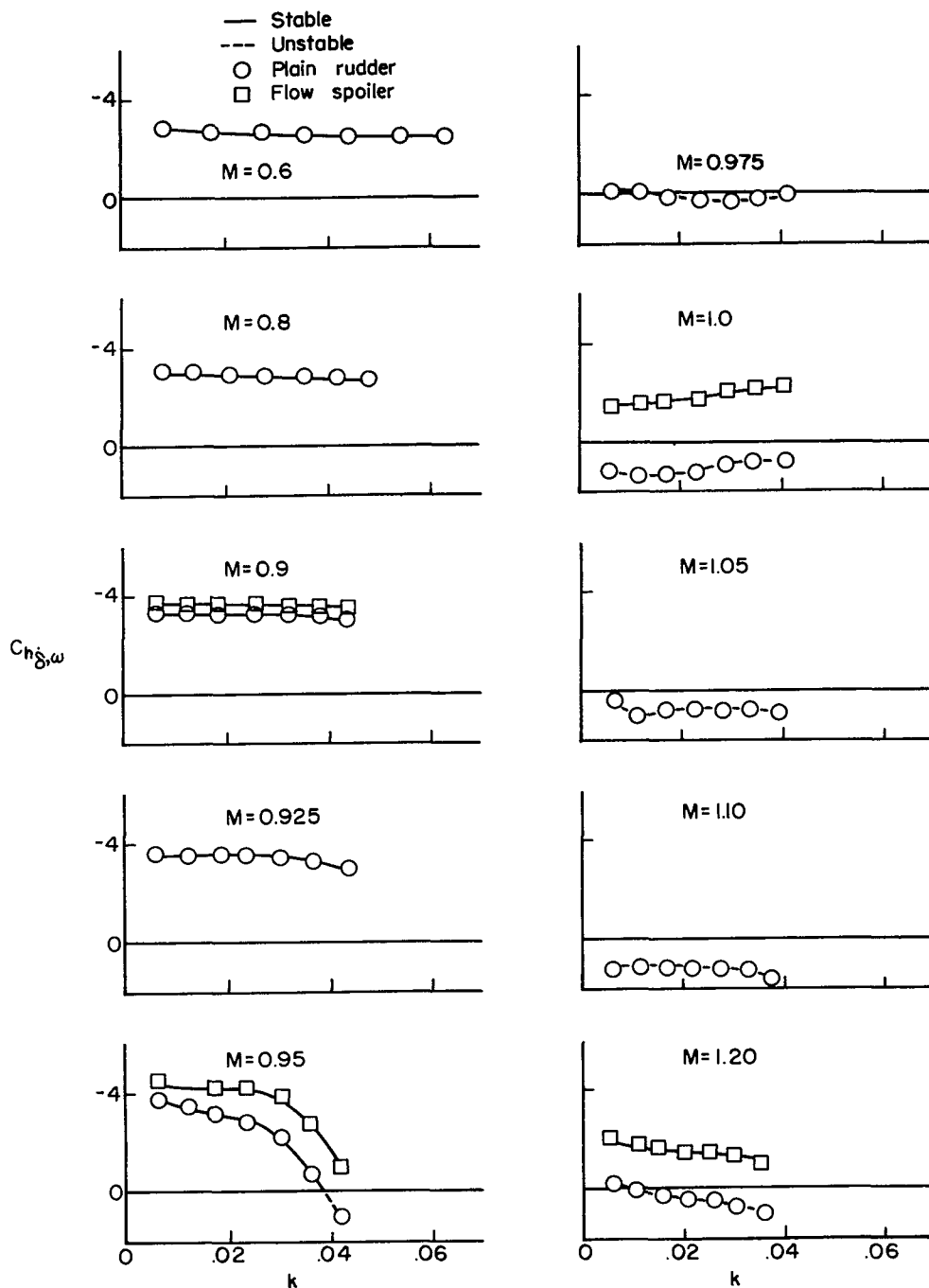


Figure 11.- Variation of  $C_{h\delta, \omega}$  with reduced frequency  $k$  for various Mach numbers showing effect of flow spoilers. Stagnation pressure, 0.70 atmosphere.

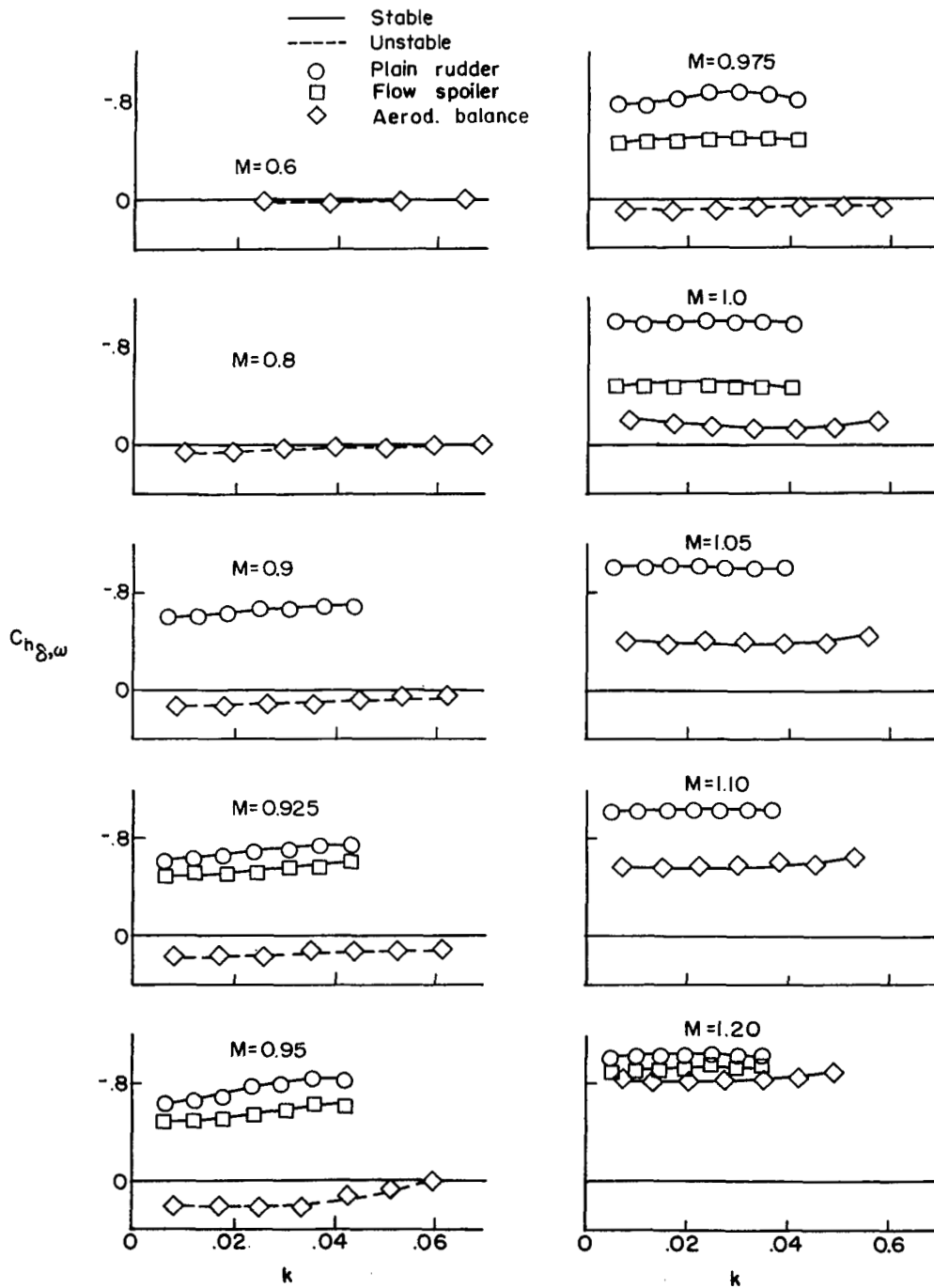


Figure 12.- Variation of  $C_{h\delta,\omega}$  with reduced frequency  $k$  for various Mach numbers showing effect of flow spoilers and aerodynamic balance. Stagnation pressure, 0.25 atmosphere.

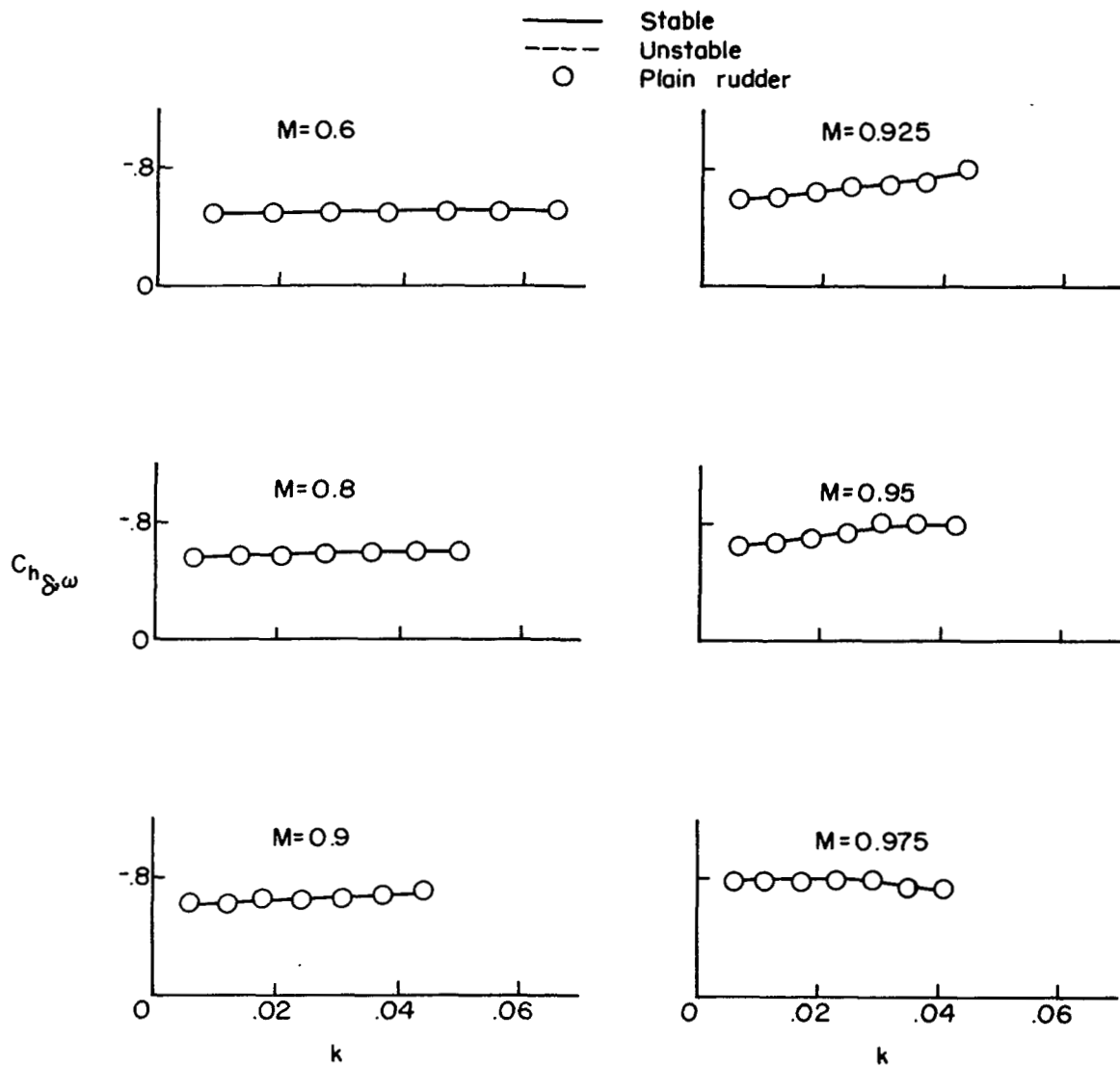


Figure 13.- Variation of  $C_{h\delta, \omega}$  with reduced frequency  $k$  for various Mach numbers. Stagnation pressure, 0.40 atmosphere.

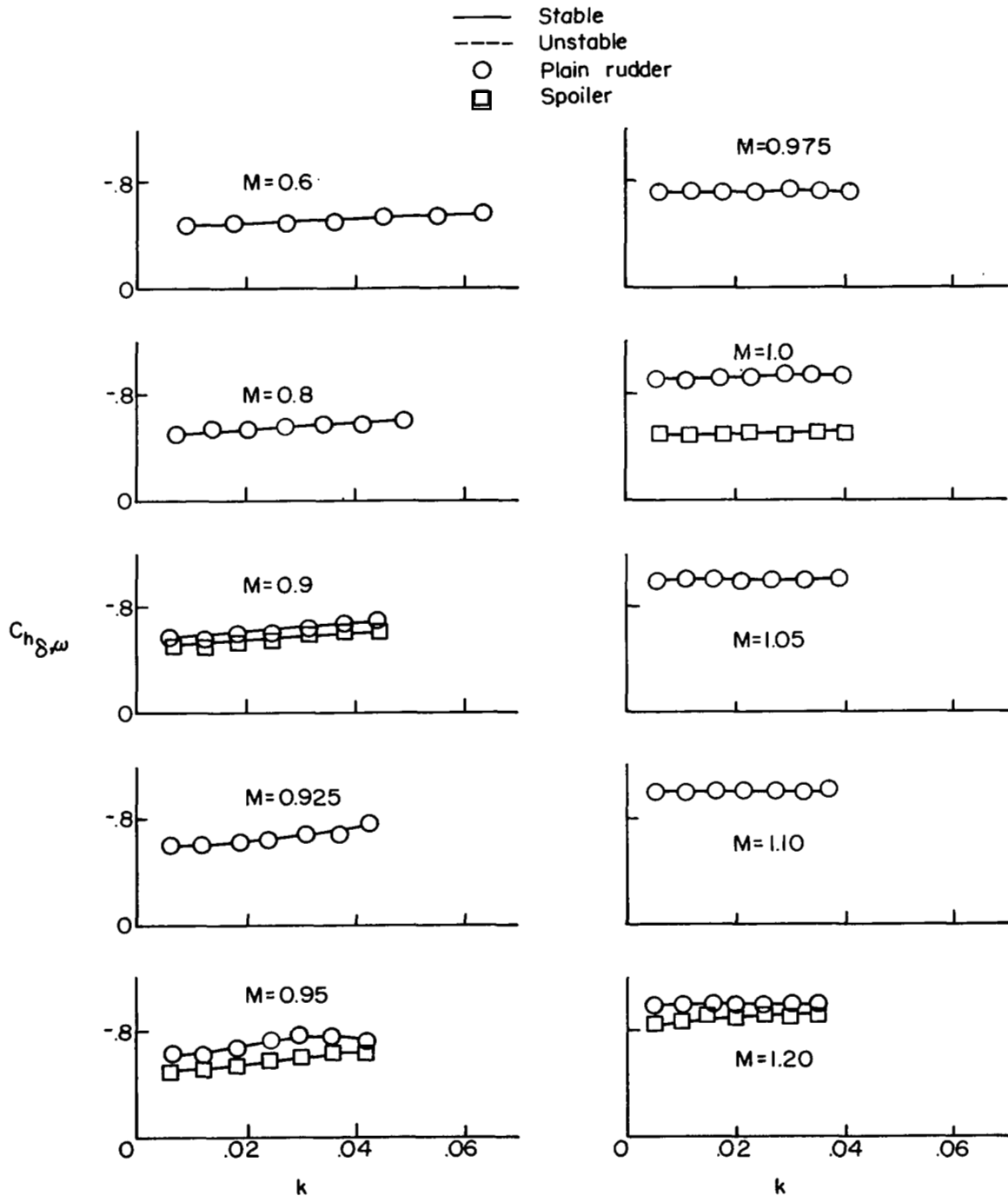


Figure 14.- Variation of  $C_{h\delta, \omega}$  with reduced frequency  $k$  for various Mach numbers showing effect of flow spoilers. Stagnation pressure, 0.70 atmosphere.

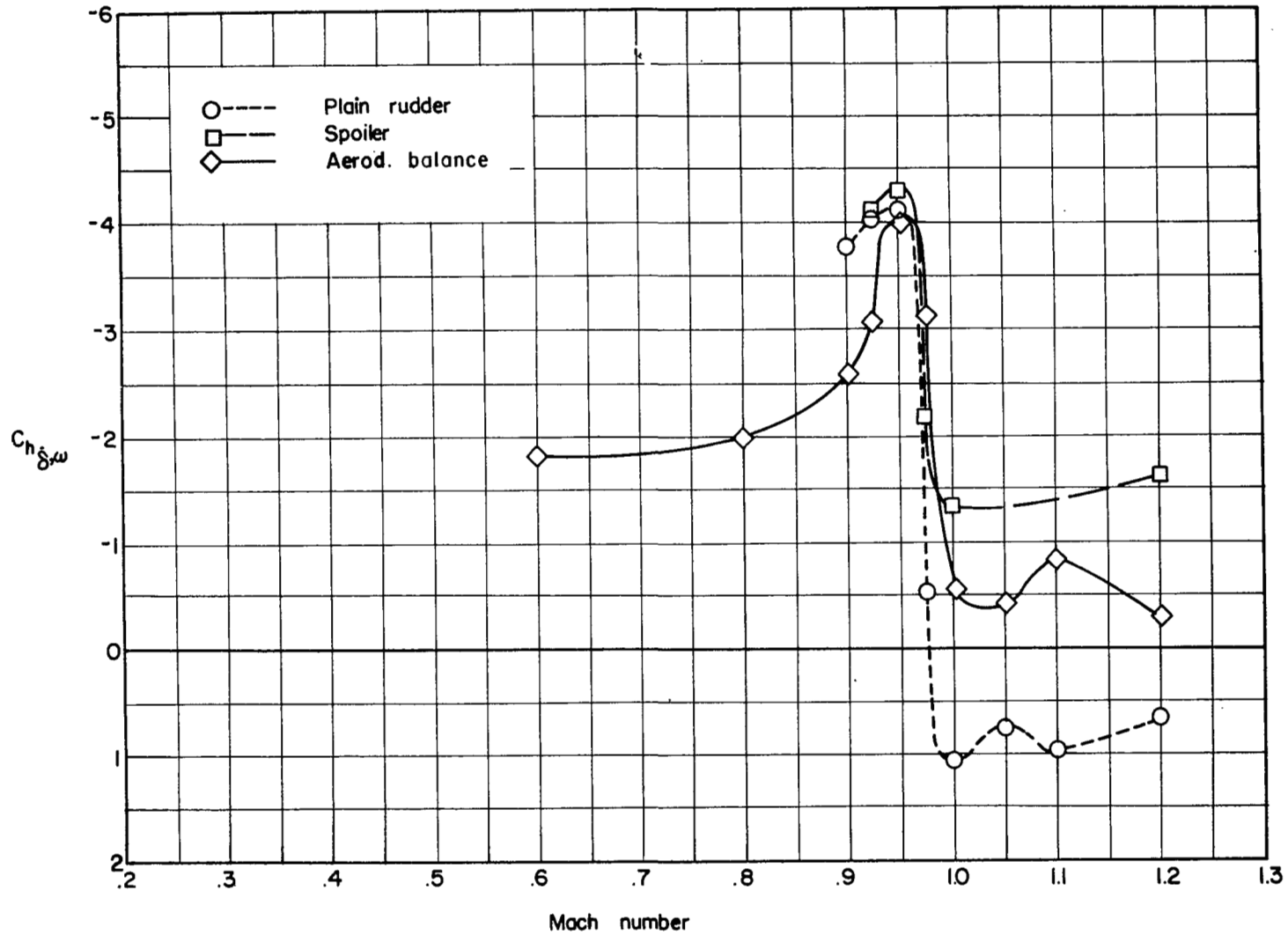


Figure 15.- Comparison of aerodynamic damping-moment coefficient of the three test configurations through the Mach number range. Stagnation pressure, 0.25 atmosphere;  $k = 0.025$ .

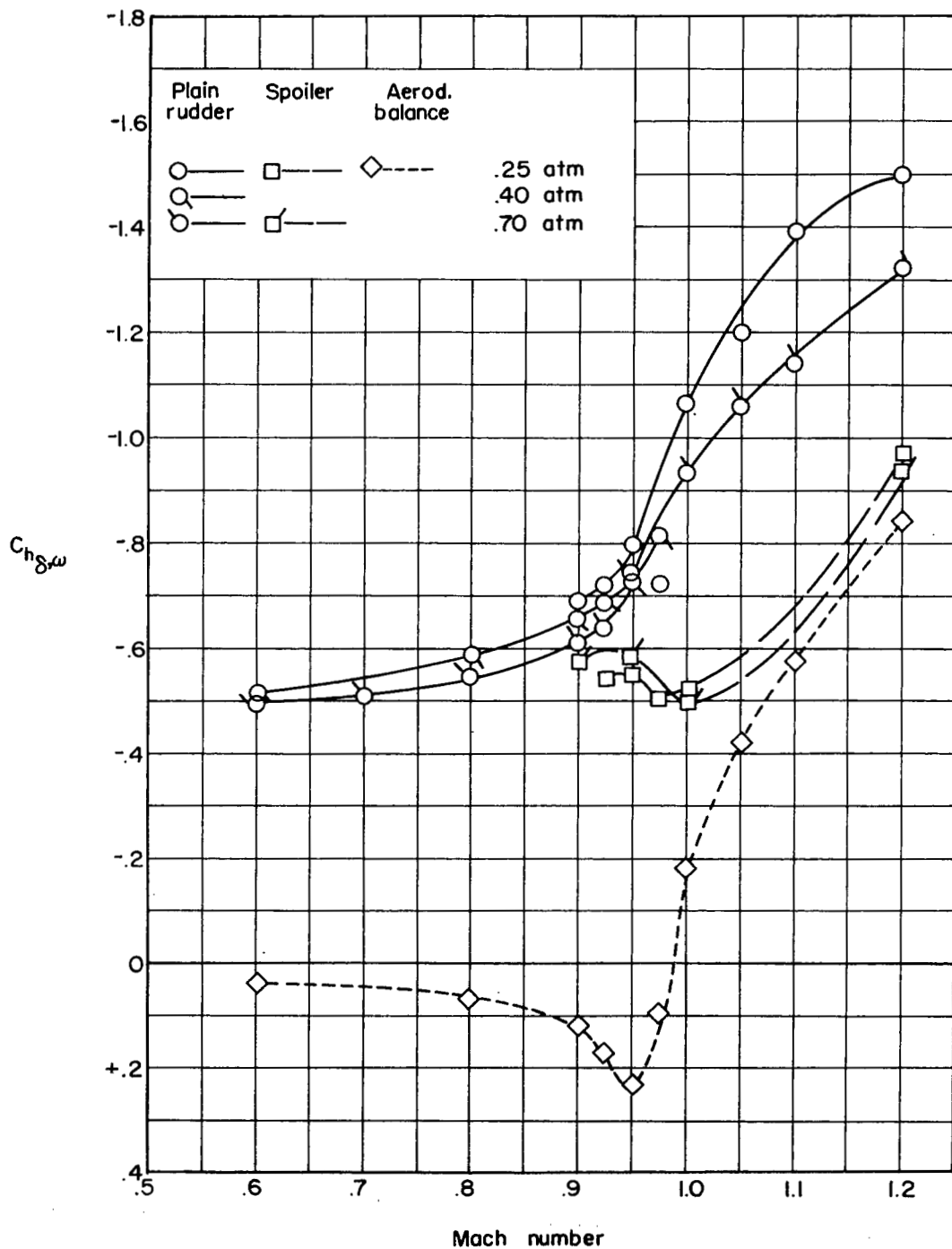


Figure 16.- Variation of the aerodynamic spring moment coefficient with Mach number for all test conditions.  $k = 0.025$ .

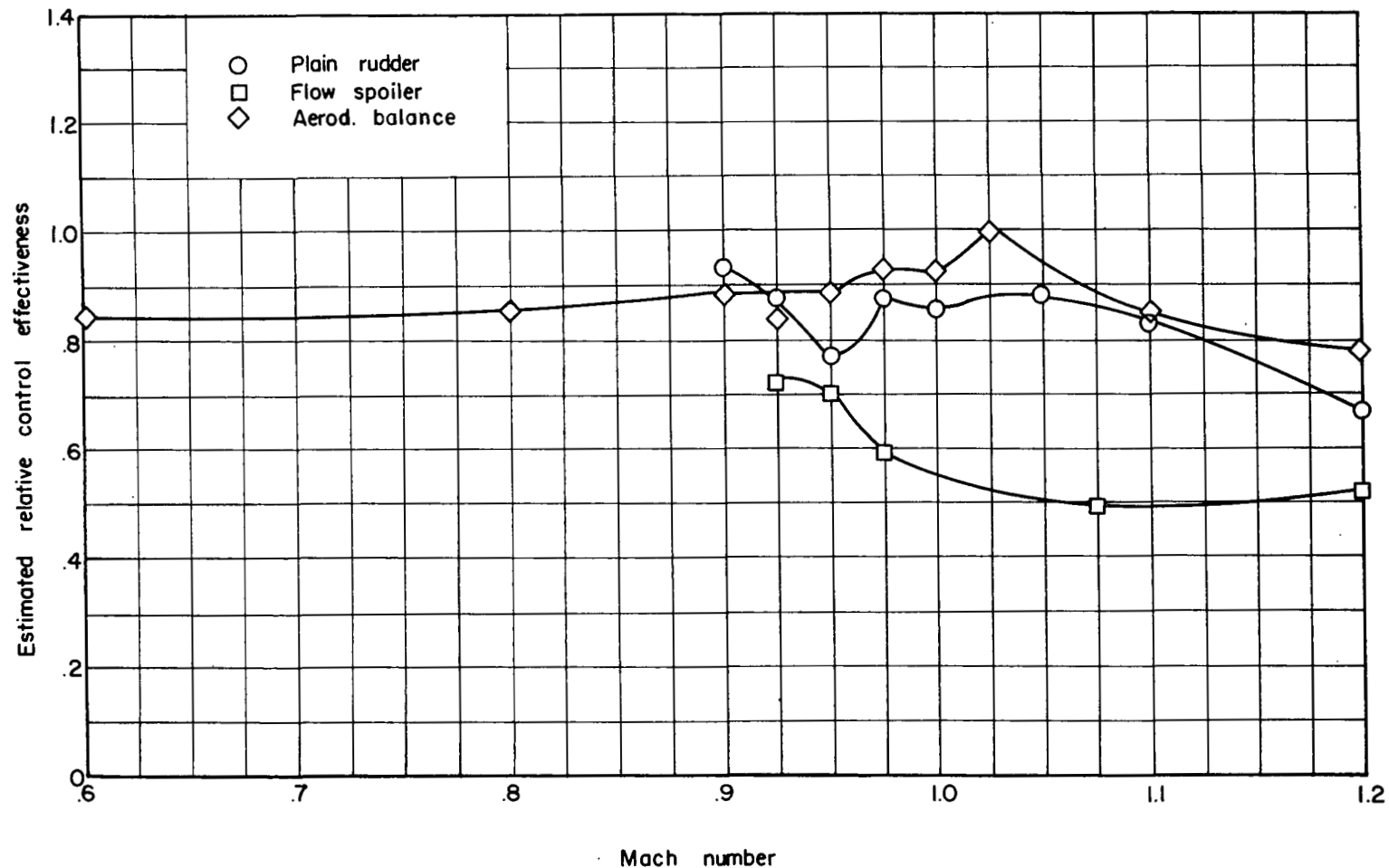


Figure 17.- Estimated relative control effectiveness of three rudder configurations through the Mach number range. Driving frequency, 5 cps.

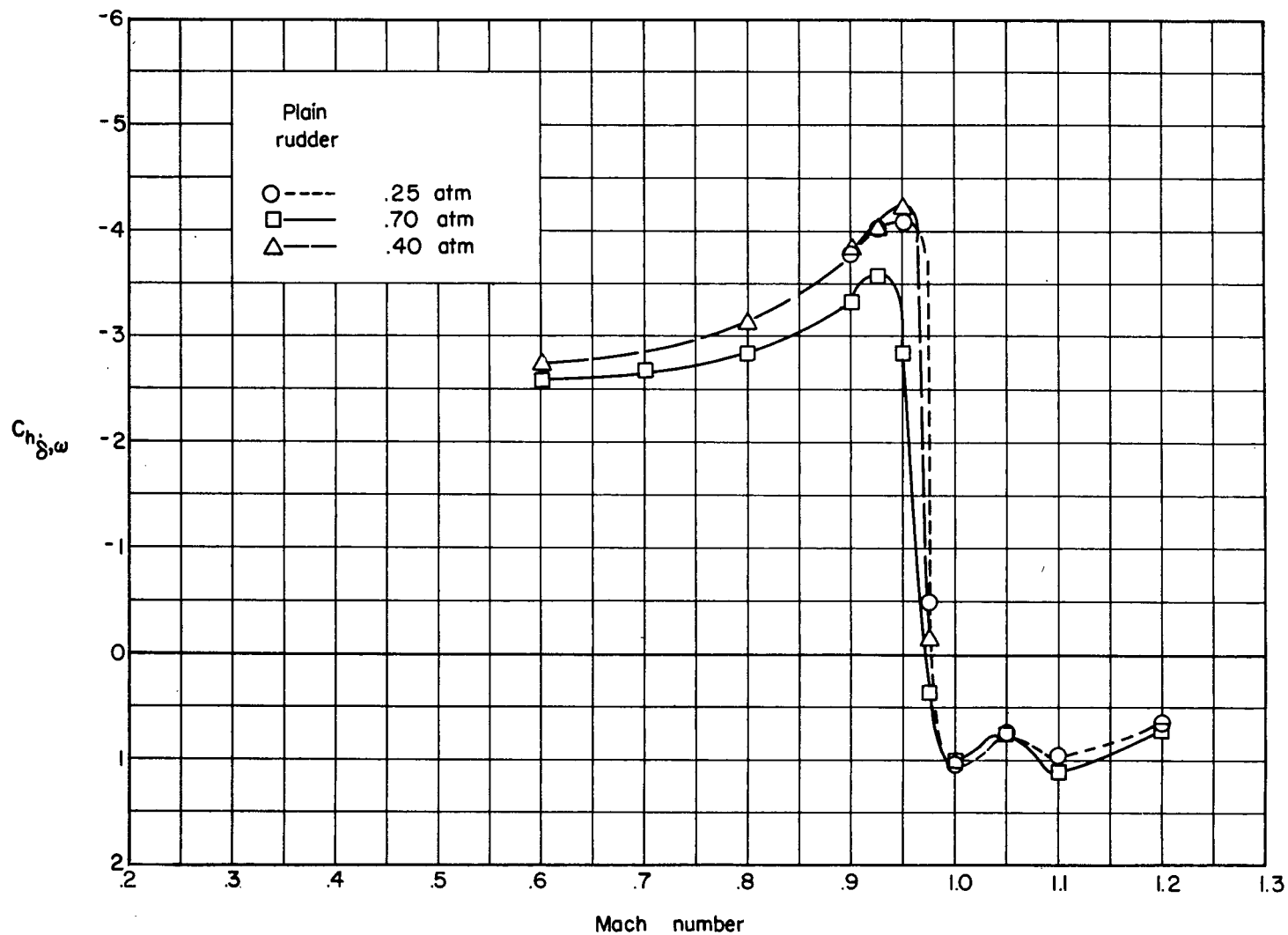


Figure 18.- Variation of aerodynamic damping-moment coefficient with Mach number for several stagnation pressures.  $k = 0.025$ .

NASA Technical Library



3 1176 01437 7874

